Applied Surface Science 454 (2018) 227–232

Contents lists available at ScienceDirect

Applied Surface Science

journal homepage: www.elsevier.com/locate/apsusc

Full Length Article

Characterization of reflow soldering at a peak temperature of 215 °C using a Bi-coated Sn-3.0Ag-0.5Cu solder ball

Jun Ho Hwang, Jong-Hyun Lee*

Department of Materials Science and Engineering, Seoul National University of Science and Technology, 232 Gongneung-ro, Nowon-gu, Seoul 139-743, Republic of Korea

ARTICLE INFO

Keywords:
Bi-coated solder ball
Low-temperature reflow soldering
Bi-coating thickness
Shear strength
Strain-rate sensitivity

ABSTRACT

Reflow soldering using a Bi-coated Sn-3.0(wt%)Ag-0.5Cu (SAC305) solder ball was successfully performed at a low peak temperature of 215 °C. The Bi shell promptly transformed into a Sn-58Bi eutectic alloy by rapid Bi diffusion into the inner SAC305 during heating, which resulted in melting at 138 °C. The bonding area on a Cu pad produced by melting increased proportionally with the initial thickness of the Bi shell. Although the overall shear force of the solder bump was lower than those of Sn-58Bi and SAC305 bumps due to the smaller bonding area, the shear force per unit area was the highest.

1. Introduction

Ever since the identification of Sn-3.0(wt%)Ag-0.5Cu (SAC305) as a viable Pb-free solder composition, Pb-free soldering technology has dominated the electronic packaging industry with relatively satisfactory properties provided by this composition [1–6]. Thus far, the extensive development of area-array-type packages has demanded that solder balls of this composition be used as typical bumping and interconnection material [4–6]. However, there is still a need for low thermal-resistance organic substrates and a reduction in the thermal degradation of devices; these demands could be met by producing a solder ball made of Pb-free solder alloys with a lower melting point. While Sn-58(wt%)Bi alloy has been considered for low melting point solders, the high-strain rate brittle fracture of joints made using the alloy and its relatively low electrical conductivity have hindered its widespread commercial use [7–12].

The various properties of solder balls are dependent on the physical and mechanical characteristics of their constituent alloy. For this reason, many studies have sought to enhance the properties of the solder by the addition of secondary materials, such as metals [13,14], intermetallic compounds (IMCs) [15,16], ceramics [17–20], carbon nanotubes [21,22], and graphene [23,24] to the alloy. However, because such addition does not change the fundamental physical properties of the matrix material, characteristics such as the high meting point of SAC305 and the electrical conductivity and strain-rate sensitivity of Sn-58Bi cannot be significantly improved.

To concurrently obtain a reduction in bonding temperature, enhancement of electrical conductivity, and mitigation of strain-rate sensitivity, we fabricated solder balls with core-shell structures. The shell was made of Bi to induce bonding by melting at a lower temperature and the core was comprised of the SAC305 alloy, which has a higher electrical conductivity than Sn-58Bi. Previous work with the goal of lowering the bonding temperature by inducing melting-point depression in the surface has involved investigation of a Sn-Bi-coated Sn-3.5Ag plate [25]. However, there were some drawbacks to this material, specifically, the Sn-Bi alloy composition is extremely sensitive to changes in current density and the material was not ball-shaped. A similar material with more practical applicability is a pure Bi-coated solder ball. Korhonen et al. prepared 1 μm-thick Bi-coated SnAg solder balls and tried to bond them with Au-finished Cu as well as Bi/Sn-finished Cu pads at various temperatures [26]. In the work, although the thermodynamic approach and phase diagrams calculations regarding the phase change by soldering were explained in detail, the study did not involve the role and optimization of the Bi-coating thickness and measurement of the bonding strength, both of which are very crucial for industrial applications. To this end, the characterization of low-temperature soldering using a Bi-coated SAC305 solder with different Bi-shell thicknesses was conducted in this study.

2. Materials and methods

The pure Bi shells on SAC305 solder balls (450 μm, MK Electron Co., Ltd) were formed by electroless plating. Prior to coating, the oxide layers on the SAC305 solder balls were removed by dipping and stirring in a pretreatment solution for 30 s. The pretreatment solution was prepared by mixing hydrochloric acid (HCl, 35.0–37.0%, Daejung Chemical) and hydrofluoric acid (HF, 48.0–51.0%, J. T. Baker) in a molar ratio of 1:1 and diluting this mixture to a concentration of 1%

* Corresponding author.
E-mail address: pljh@snut.ac.kr (J.-H. Lee).

https://doi.org/10.1016/j.apsusc.2018.05.129
Received 24 April 2018; Accepted 17 May 2018
Available online 19 May 2018

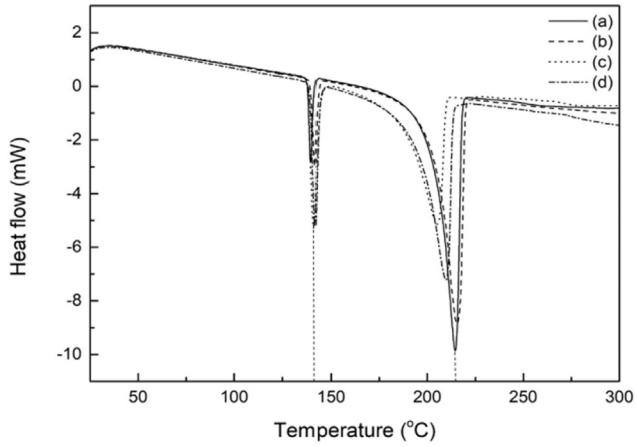

Fig. 1. DSC results of Bi-coated SAC305 solder balls prepared with different Bi thicknesses: (a) 1.7, (b) 3.4, (c) 7.0, and (d) 12.0 μm.

using distilled water. Immediately after pretreatment, Bi shells were fabricated by dipping and stirring the washed solder balls in a Bi plating solution. The Bi plating solution consisted of 0.08 M bismuth(III) chloride ($BiCl_3$, 97.0%, Junsei Chemical), 0.2 M nitrilotriacetic acid ($(CH_2COOH)_3$, 98.0%, Junsei Chemical), 0.34 M sodium citrate ($C_6H_5Na_3O_7{\cdot}2H_2O$, 99.0%, Susin Chemical), 0.08 M ethylenediaminetetraacetic acid ($C_{10}H_{16}N_2O_8$, 99.0%, Susin Chemical), and 0.313 M sodium phosphate monohydrate ($NaH_2PO_2{\cdot}H_2O$, 98.0%, Kishida Chemical) with 30 ml of distilled water. The pH value of the mixed solution was adjusted to 8.75 by adding ammonia solution while stirring at 50 °C for 1 h. SAC305 solder balls (0.15 g) were dipped and stirred in the plating solution for four different plating times of 5, 10, 15, and 20 min to fabricate Bi shells of different thicknesses. Finally, the Bi-coated SAC305 solder balls were washed with distilled water three times and dried.

The melting and thermal properties of the fabricated solder balls were investigated using a differential scanning calorimeter (DSC, DSC-60, Shimadzu). The cross-sectional microstructures of solder balls and solder bumps formed on pads were imaged using a scanning electron microscope (SEM, VEGA 3 LMU, TESCAN). As the pad material, organic solderability preservative (OSP)-coated Cu was used. To analyze, in detail, the change in the elemental content on the bonding interface, an electron probe microanalyzer (EPMA, JXA-8530F, JEOL) was used. The solderability of the fabricated solder balls was quantitatively evaluated by shear testing the bumps formed after reflow soldering. For comparison, Sn-58Bi (450 μm, Duksan Hi-Metal Co., Ltd) and SAC305 solder balls were also evaluated. The peak temperatures for the reflow bumping were different for the different materials: 181 °C for Sn-58Bi,

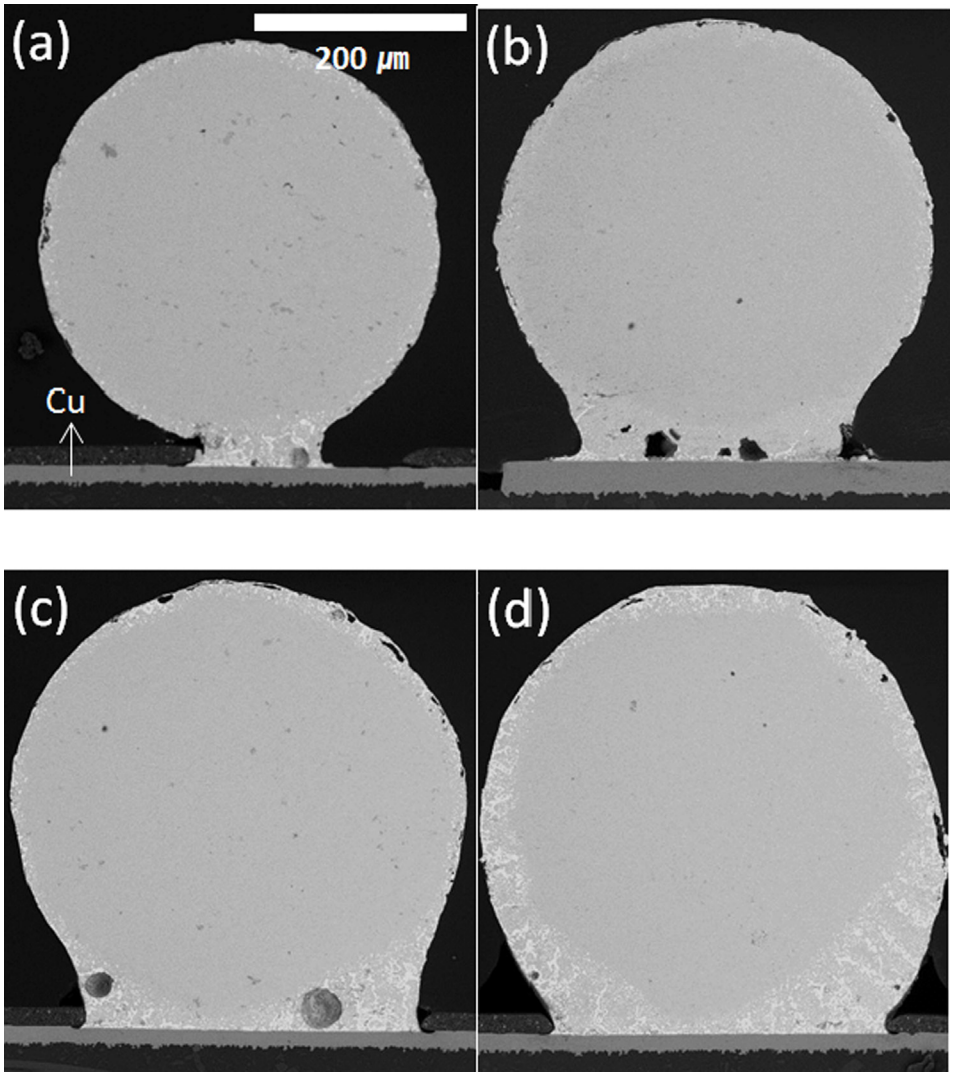

Fig. 2. Cross-sectional SEM images of Bi-coated SAC305 solder balls obtained before and after reflow soldering at 215 °C with different thicknesses of Bi shell: (a) 1.7, (b) 3.4, (c) 7.0, and (d) 12.0 μm.

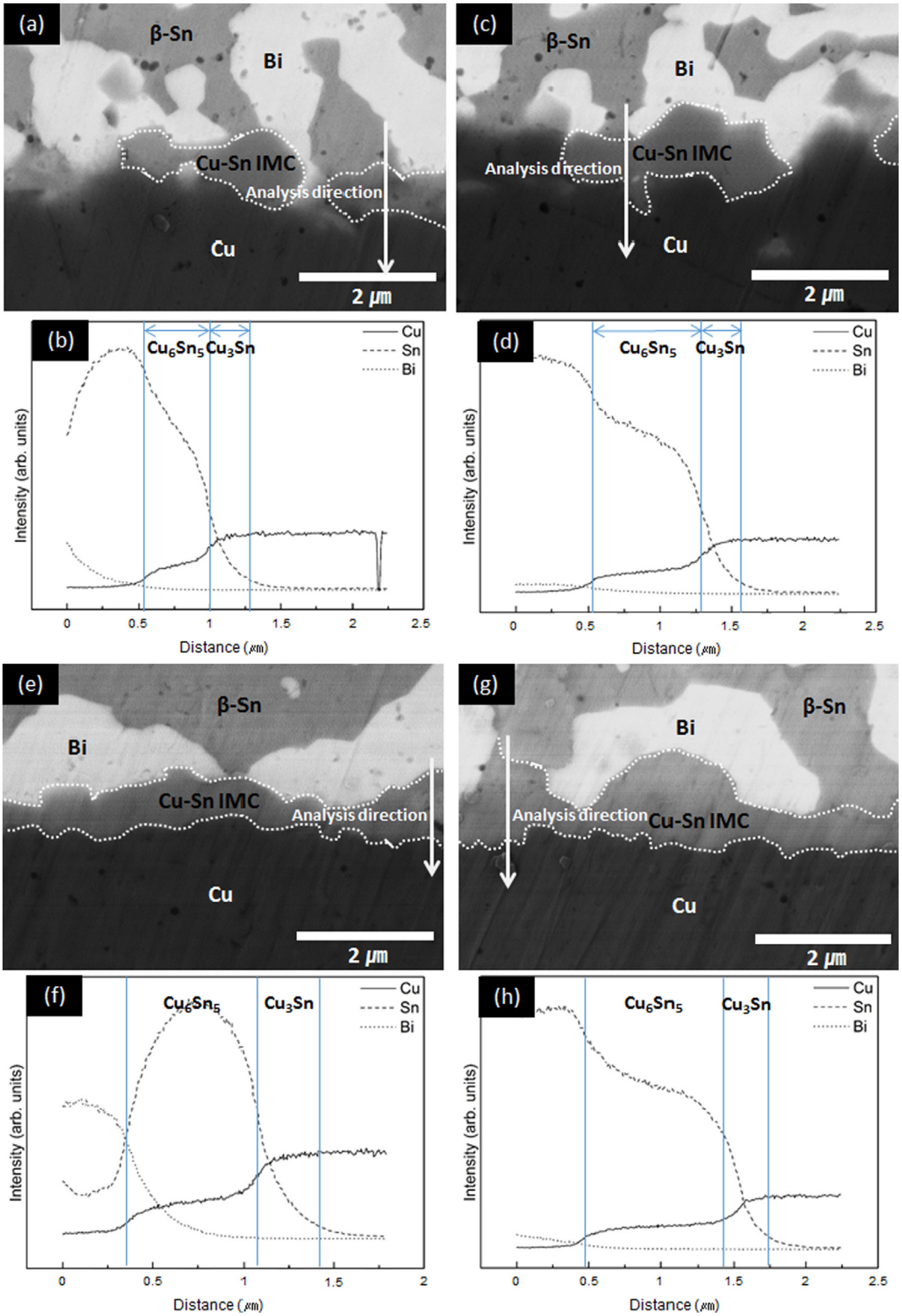

Fig. 3. (a, c, e, g) Cross-sectional SEM images and (b, d, f, h) EPMA results taken at the Bi-coated SAC305 solder ball/Cu pad interface after reflow at 215 °C with different thicknesses of Bi shell: (a) 1.7, (b) 3.4, (c) 7.0, and (d) 12.0 μm. Note that the formed Cu-Sn IMC was discontinuous when the Bi thickness was 1.7 and 3.4 μm and the IMC consisted of Cu_6Sn_5 and Cu_3Sn in all samples.

215 °C for Bi–coated SAC 305, and 249 °C for SAC305. Bump shear tests were conducted using a speed-adjustable bond tester (DAGE-4000HS, Nordson DAGE) at a fixed shear height of 50 μm. One hundred samples were tested under each condition, and the average values are reported.

3. Results and discussion

Fig. 1 shows the DSC results from Bi-coated SAC305 solder balls at various average thicknesses of the initial Bi shell when they were heated up to 300 °C at a heating rate of 10 °C/min. The most striking result

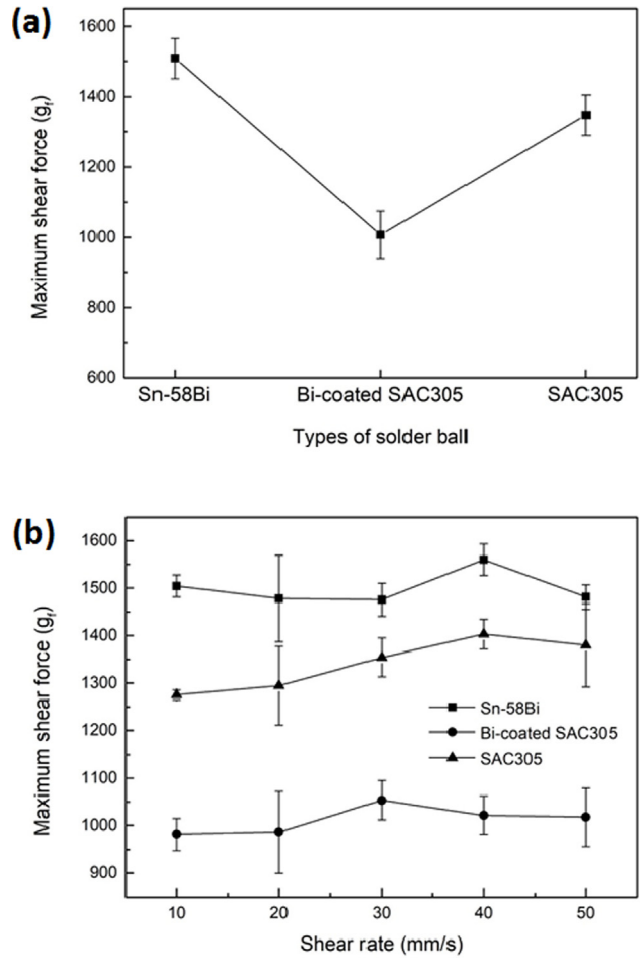

Fig. 4. (a) Maximum shear force before failure measured after reflow soldering of various solder balls of 450 μm and (b) maximum shear force measured as a function of shear rate.

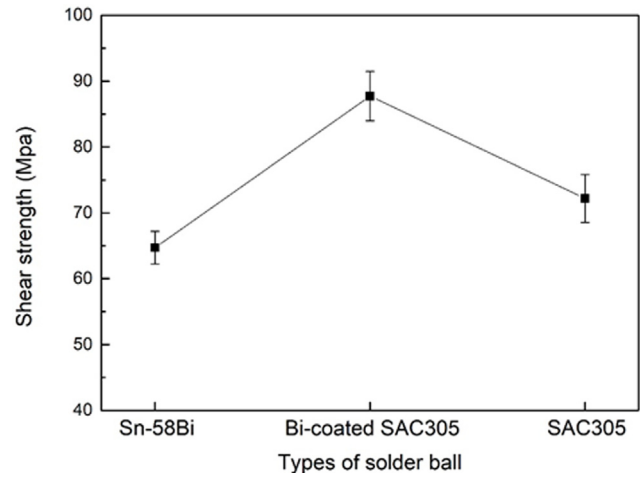

Fig. 5. Area-normalized shear force (shear strength) values of the bonded three-type solder balls.

was the endothermic peak near 138 °C for all four solder balls types, which suggests the in situ formation of a eutectic Sn-58Bi composition on the skin of the solder ball by fast Bi diffusion into the inner SAC305 alloy [27]. The size of the peak was proportional to the Bi thickness, meaning that the volume of formed Sn-58Bi alloy evidently increased with increasing Bi volume. An additional endothermic peak near 217 °C, the melting point of SAC305, was also observed for all solder balls. However, the latter endothermic peaks were not as sharp as the low-temperature peaks, especially with regards to the approach shape. Further, with increasing Bi thickness, the peaks moved to slightly lower temperatures and exhibited more rapidly occurring endothermic phenomena in the low-temperature tail of the peak, implying that the ternary composition of Sn-Ag-Cu transformed into quaternary compositions of Sn-Ag-Cu-Bi with Bi diffusion into the core SAC 305 [28,29].

Cross-sectional SEM images of the four-types of Bi-coated SAC305 solder balls before and after the reflow soldering at a peak temperature of 215 °C are presented in Fig. 2. The bonding area of the solder ball on an OSP/Cu pad (obtained by surface melting) increased proportionally as the Bi shell thickness increased, although the inevitable formation of pores by the evaporation of the solvent in the flux was observed in the bonding region. Another impressive result is that a large amount of the molten skin was transferred to the interface between the solder ball and the OSP/Cu pad by flow under gravity. Consequently, this phenomenon increased the final volume of molten Sn-Bi in the bonding region. The increased volume of molten Sn-Bi eventually eroded away the core SAC solder near the interface.

Fig. 3 shows cross-sectional SEM images and EPMA results of the Bi-coated SAC305 solder ball/Cu pad interface after reflow at 215 °C at various Bi shell thicknesses. For all thickness values, a Cu-Sn IMC was formed between the solder ball and the Cu pad although the IMC was discontinuous when the Bi thickness was 1.7 and 3.4 μm. The continuity and average thickness of the IMC increased proportionally with increasing Bi thickness. From the EPMA results, it was found that the IMC consisted of Cu_6Sn_5 and Cu_3Sn although there were drastic compositional changes within the IMCs as they were very thin [30]. These results imply that the bumping process on a Cu pad using the Bi-coated SAC305 solder ball mitigates the excessive growth of IMCs that has been reported to be detrimental to the reliability of the solder joint [31–35]. Since Sn is consumed to form the Cu-Sn IMC, the composition of the molten Sn-Bi alloy will transfer into a hypereutectic one (Bi-rich composition). This IMC, which is comprised of the two phases Cu_6Sn_5 and Cu_3Sn, grows from a discontinuous to a continuous layer with increasing thickness of the Bi shell.

Fig. 4a shows the maximum shear force values before failure measured after the reflow bonding of three-types of solder balls (Bi-coated SAC305, Sn-58Bi, and SAC305), each with diameters of 450 μm. The thickness of the Bi shell in the Bi-coated SAC305 solder ball was 12.0 μm. Of the average value of forces measured at all shear rates from 10 to 50 mm/s, the force of Sn-58Bi solder ball, which had the largest bonding area, was the highest at 1508 g_f. The average bonding areas were measured to be 0.229, 0.183, and 0.115 mm^2 for Sn-58Bi, SAC305, and Bi-coated SAC305, respectively. The force of the Bi-coated SAC305 solder balls was the lowest due to its much smaller bonding area compared with the Sn-58Bi and SAC305 solder balls. The reduced bonding area can be directly linked to a decrease in shear force of the bonded solder ball. Detailed plots of the maximum shear force versus the shear rate are displayed in Fig. 4b. We note again that at all shear rates from 10 to 50 mm/s, Sn-58Bi solder balls showed the highest maximum shear force value and Bi-coated SAC305 solder balls showed the lowest.

Since the low shear forces of Bi-coated SAC305 solder balls were attributed to their reduced bonding areas, their shear force values were normalized by their bonding areas to compare the shear force values per unit area. Fig. 5 represents the area-normalized shear force (shear strength) values of bonded three-type solder balls. Interestingly, the shear strength of the Sn-58Bi solder balls divided by area was the smallest in value. In contrast, the area-normalized shear strength value of the Bi-coated SAC305 solder balls was the highest. This result means that bonding of the Bi-coated SAC305 solder ball was the best of the different materials for identical bonding areas. As mentioned earlier, the Bi content in the bonding region increases due to consumption of Sn by the formation of a Cu-Sn IMC, and it has been reported that

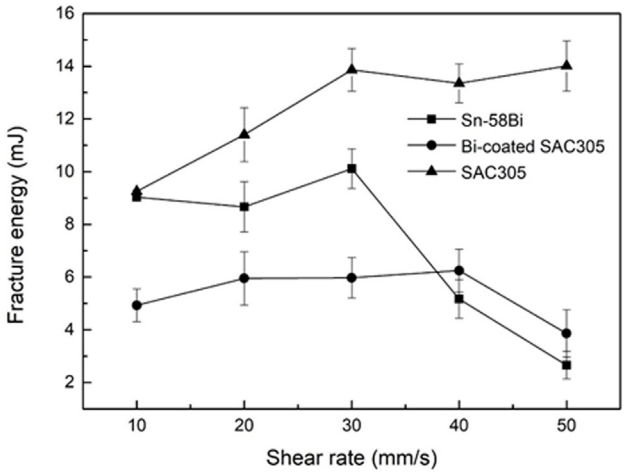

Fig. 6. Fracture energy of the bonded three-type solder balls measured as a function of shear rate.

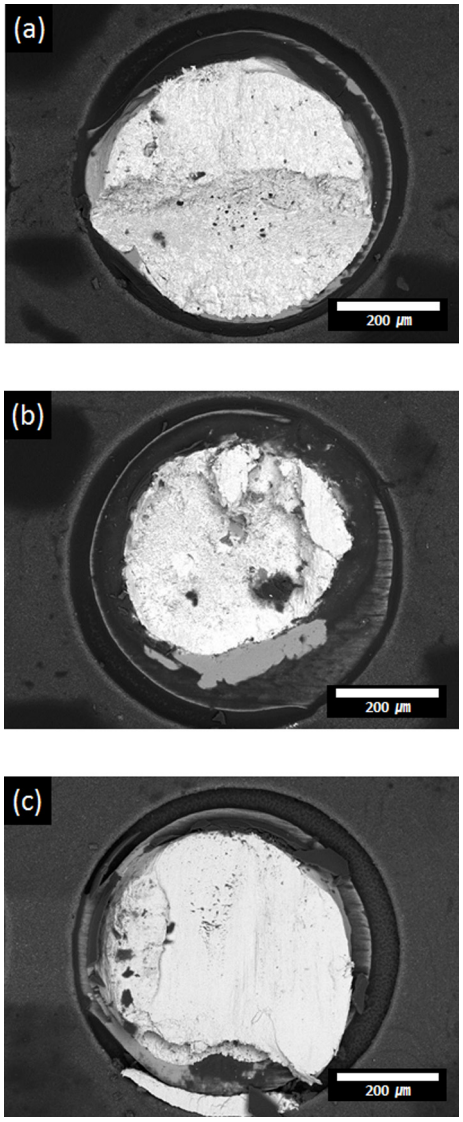

Fig. 7. Representative fracture surfaces observed after shear testing: (a) Sn-58Bi, (b) Bi-coated SAC305, and (c) SAC305 solder bumps.

increased Bi content in Sn-Bi increases the strength of the alloy [36].

Lastly, the change in the fracture energy measured as a function of shear rate is shown in Fig. 6. With an increase in the shear rate, the fracture energy of the SAC305 solder increased. However, the fracture energy of Sn-58Bi drastically decreased due to the brittle fracture characteristic of low elongation behavior in the shear rate range of 30–40 mm/s, due to its sensitivity to high strain rate. While the fracture energy of the Bi-coated SAC305 solder ball was the lowest up to a shear rate of 30 mm/s, the decrease in its fracture energy was relatively low in the range of 30–50 mm/s, implying that the strain-rate sensitivity was mitigated in comparison with that of pure Sn-58Bi. As a result, the energy value of the Bi-coated SAC305 was higher than that of Sn-58Bi from the shear rate of 40 mm/s, with lower brittle fracture behavior despite its inherently small bonding area.

Fig. 7 shows the representative fracture surfaces observed after shear testing. Despite significantly reduced bonding area, the fracture surfaces created after reflow bonding of a Bi-coated SAC305 ball presented ductile fracture in the solder bump, just like the results observed in the bumps fabricated with Sn-58Bi and SAC305 solder balls. This fracture characteristic indicates that the reflow bonding using Bi-coated SAC305 balls proceeds as a normal soldering process.

We believe that this Bi-coated SAC305 solder ball is a potentially useful material for solder bumps of a uniform height required in a package stacking process for the construction of a package on package structure because of the partial melting that occurs only at the surface. It may also be used as a higher solder bump obtained through partial melting of the surface in an identical pad size for the establishment of more reliable bonding in a device mounting process.

4. Conclusions

Low-temperature reflow soldering using a Bi-coated SAC305 solder ball was successfully demonstrated at a peak temperature of 215 °C. With the rapid diffusion of Bi to the inner SA305 during the heating, the Bi shell immediately transformed into a Sn-58Bi eutectic alloy, which induced melting at 138 °C and initiated wetting on a Cu pad at higher temperatures. With an increase in the initial thickness of the Bi shell, the volume of the molten alloy on the surface increased, along with the bonding area. The Cu-Sn IMC growth at the interface of the solder ball/Cu pad also accelerated due to the transportation of the molten alloy to the bonding region on the pad by flow under gravity. The maximum shear force of the joint reflow-bonded by the Bi-coated SAC305 solder ball was lower than those of joints formed by Sn-58Bi and SAC305 due to its small bonding area, however, the shear force per unit area of the Bi-coated SAC305 was the highest. Moreover, the strain-rate sensitivity leading to brittle fracture, a crucial problem observed in Sn-58Bi alloys, was mitigated in the Bi-coated SAC305 solder ball.

Acknowledgements

The authors thank the Korean Basic Science Institute (KBSI), Busan Center for the thermogravimetric analysis.

References

[1] Y.-C. Lin, J.-G. Duh, Phase transformation of the phosphorus-rich layer in SnAgCu/Ni–P solder joints, Scr. Mater. 54 (2006) 1661–1665.
[2] G. Zeng, S. Xue, L. Zhang, L. Gao, W. Dai, J. Luo, A review on the interfacial intermetallic compounds between Sn–Ag–Cu based solders and substrates, J. Mater. Sci. Mater. Electron. 21 (2010) 421–440.
[3] V.M.F. Marques, C. Johnston, P.S. Grant, Nanomechanical characterization of Sn–Ag–Cu/Cu joints—Part 1: Young's modulus, hardness and deformation mechanisms as a function of temperature, Acta Mater. 61 (2013) 2460–2470.
[4] S. Kumamoto, H. Sakurai, Y. Kukimoto, K. Suganuma, Joint strength and microstructure for Sn-Ag-(Cu) soldering on an electroless Ni-Au surface finish by using a flux containing a Cu compound, J. Electron. Mater. 37 (2008) 806–814.
[5] J.-W. Yoon, B.-I. Noh, Y.-H. Lee, H.-S. Lee, S.-B. Jung, Effects of isothermal aging and temperature–humidity treatment of substrate on joint reliability of Sn–3.0Ag–0.5Cu/OSP-finished Cu CSP solder joint, Microelectron. Reliab. 48

(2008) 1864–1874.
[6] Y.-H. Baek, B.-M. Chung, Y.-S. Choi, J. Choi, J.-Y. Huh, Effects of Ni_3Sn_4 and (Cu, Ni_j6S_n5 intermetallic layers on cross-interaction between Pd and Ni in solder joints, J. Alloys Compd. 579 (2013) 75–81.
[7] M. Mccormack, H.S. Chen, G.W. Kammlott, S. Jin, Significantly improved mechanical properties of Bi-Sn solder alloys by Ag- doping, J. Electron. Mater. 26 (1997) 954–958.
[8] F. Hua, Z. Mei, J. Glazer, A. Lavagnino, Eutectic Sn–Bi as an alternative to Pb-free solders, in: Proc. 48th Electronic Components and Technology Conference (ECTC), IEEE, New Jersey, 1998, pp. 277–283.
[9] S. Kikuchi, M. Nishimura, K. Suetsugu, T. Ikari, K. Matsushige, Strength of bonding interface in lead-free Sn alloy solders, Mat. Sci. Eng. A 319 (2001) 475–479.
[10] K. Suganuma, T. Sakai, K.-S. Kim, Y. Takagi, J. Sumimoto, M. Ueshima, Thermal and mechanical stability of soldering QFP with Sn–Bi–Ag lead-free alloy, IEEE T. Electron. Pack. 25 (2002) 257–261.
[11] W. Dong, Y. Shi, Z. Xia, Y. Lei, F. Guo, Effects of trace amounts of rare earth additions on microstructure and properties of Sn-Bi-based solder alloy, J. Electron. Mater. 37 (2008) 982–991.
[12] Y. Shiue, T. Chuang, Effect of La addition on the interfacial intermetallics and bonding strengths of Sn–58Bi solder joints with Au/Ni/Cu pads, J. Alloys Compd. 491 (2010) 610–617.
[13] A.S.M.A. Haseeb, T.S. Leng, Effects of Co nanoparticle addition to Sn–3.8Ag–0.7Cu solder on interfacial structure after reflow and ageing, Intermetallics 19 (2011) 707–712.
[14] S.L. Tay, A.S.M.A. Haseeb, M.R. Johan, P.R. Munroe, M.Z. Quadir, Influence of Ni nanoparticle on the morphology and growth of interfacial intermetallic compounds between Sn–3.8Ag–0.7Cu lead-free solder and copper substrate, Intermetallics 33 (2013) 8–15.
[15] J.-H. Lee, D.-J. Park, J.-N. Heo, Y.-H. Lee, D.-H. Shin, Y.-S. Kim, Reflow characteristics of Sn-Ag matrix in-situ composite solders, Scr. Mater. 42 (2000) 827–831.
[16] S.T. Kao, Y.C. Kin, J.G. Duh, Controlling intermetallic compound growth in SnAgCu/Ni-P solder joints by nanosized Cu_6Sn_5 addition, J. Electron. Mater. 35 (2006) 486–493.
[17] J. Shen, Y.C. Liu, Y.J. Han, Y.M. Tian, H.X. Gao, RETRACTED: Strengthening effects of ZrO_2 nanoparticles on the microstructure and microhardness of Sn–3.5Ag lead-free solder, Mater. Sci. Eng. A 441 (2006) 135–141.
[18] P. Liu, P. Yao, J. Liu, Effect of SiC nanoparticle additions on microstructure and microhardness of Sn-Ag-Cu solder alloy, J. Electron. Mater. 37 (2008) 874–879.
[19] L.C. Tsao, Suppressing effect of 0.5 wt.% nano-TiO_2 addition into Sn–3.5Ag–0.5Cu solder alloy on the intermetallic growth with Cu substrate during isothermal aging, J. Alloys Compd. 509 (2011) 8441–8448.
[20] S.Y. Chang, C.C. Jain, T.H. Chuang, L.P. Feng, L.C. Tsao, Effect of addition of TiO_2 nanoparticles on the microstructure, microhardness and interfacial reactions of Sn3.5AgXCu solder, Mater. Des. 32 (2011) 4720–4727.
[21] S.M.L. Nai, J. Wei, M. Gupta, Improving the performance of lead-free solder reinforced with multi-walled carbon nanotubes, Mater. Sci. Eng. A 423 (2006) 166–169.
[22] S. Xu, Y.C. Chan, K. Zhang, K.C. Yung, Interfacial intermetallic growth and mechanical properties of carbon nanotubes reinforced Sn3.5Ag0.5Cu solder joint under current stressing, J. Alloys Compd. 595 (2014) 92–102.
[23] X.D. Liu, Y.D. Han, H.Y. Jing, J. Wei, L.Y. Xu, Effect of graphene nanosheets reinforcement on the performance of Sn–Ag–Cu lead-free solder, Mater. Sci. Eng. A 562 (2013) 25–32.
[24] G. Chen, F. Wu, C. Liu, V.V. Silberschmidt, Y.C. Chan, Microstructures and properties of new Sn–Ag–Cu lead-free solder reinforced with Ni-coated graphene nanosheets, J. Alloys Compd. 656 (2016) 500–509.
[25] J. Lee, W. Bang, J. Jung, K. Oh, Microstructure and strength of Sn-Bi coated Sn-3.5 mass%Ag solder alloy, Mater. Trans. 45 (2004) 783–789.
[26] T.-M. Korhonen, V. Vuorinen, J.K. Kivilahti, Interconnections based on Bi-coated SnAg solder balls, IEEE Trans. Adv. Packag. 24 (2001) 515–520.
[27] A.M. Delhaise, D.D. Perovic, Study of solid-state diffusion of Bi in polycrystalline Sn using electron probe microanalysis, J. Electron. Mater. 47 (2018) 2057–2065.
[28] J. Zhao, L. Qi, X. Wang, L. Wang, Influence of Bi on microstructures evolution and mechanical properties in Sn–Ag–Cu lead-free solder, J. Alloys Compd. 375 (2004) 196–201.
[29] J. Zhao, Y. Mutoh, Y. Miyashita, S.L. Mannan, Fatigue crack-growth behavior of Sn-Ag-Cu and Sn-Ag-Cu-Bi lead-free solders, J. Electron. Mater. 31 (2002) 879–886.
[30] J. Gong, C. Liu, P.P. Conway, V.V. Silberschmidt, Evolution of CuSn intermetallics between molten SnAgCu solder and Cu substrate, Acta Mater. 56 (2008) 4291–4297.
[31] D.R. Frear, P.T. Vianco, Intermetallic growth and mechanical behavior of low and high melting temperature solder alloys, Metall. Mater. Trans. A 25 (1994) 1509–1523.
[32] L. Xu, J.H.L. Pang, F. Che, Impact of thermal cycling on Sn-Ag-Cu solder joints and board-level drop reliability, J. Electron. Mater. 37 (2008) 880–886.
[33] Y.-C. Chiou, Y.-M. Jen, S.-H. Huang, Finite element based fatigue life estimation of the solder joints with effect of intermetallic compound growth, Microelectron. Reliab. 51 (2011) 2319–2329.
[34] F.X. Che, J.H.L. Pang, Characterization of IMC layer and its effect on thermo-mechanical fatigue life of Sn–3.8Ag–0.7Cu solder joints, J. Alloys Compd. 541 (2012) 6–13.
[35] T. An, F. Qin, Effects of the intermetallic compound microstructure on the tensile behavior of Sn3.0Ag0.5Cu/Cu solder joint under various strain rates, Microelectron. Reliab. 54 (2014) 932–938.
[36] H. Takao, A. Yamada, H. Hasegawa, Development of wettability evaluation technique applying contact angle measurement during soldering, R&D Review of Toyota CRDL 39 (2004) 41–48.